

Supporting Information for

Regulating the structural dimensionality and dynamic properties of a porous dysprosium coordination polymer through solvent molecules

Fang Ma,^a Rong Sun,^b Ai-Huan Sun,^a Jin Xiong,^b Hao-Ling Sun,*^a and Song Gao*^b

^a Department of Chemistry and Beijing Key Laboratory of Energy Conversion and Storage Materials, Beijing Normal University, Beijing 100875, P. R. China. E-mail: haolingsun@bnu.edu.cn;

^b Beijing National Laboratory for Molecular Sciences, State Key Laboratory of Rare Earth Materials Chemistry and Applications, College of Chemistry and Molecular Engineering, Peking University, Beijing 100871, China. E-mail: gaosong@pku.edu.cn;

Experimental Section

X-ray crystallography and physical measurement

Intensity data for crystals of **1** and **2** were collected on a rigaku SuperNova, Dual, AtlasS2 diffractometer with graphite-monochromated Cu K α radiation at 100 K. Using Olex2, the structure was solved with the olex2. solve structure solution program using Charge Flipping and refined with the olex2. refine refinement package using Gauss-Newton minimisation. All non-hydrogen atoms were refined anisotropically. Hydrogen atoms were placed at the calculation positions. The details of crystallographic data and selected bond parameters for complexes **1** and **2** are listed in Table S1, respectively.

Elemental analyses of carbon, hydrogen, and nitrogen were carried out with an Elementar Vario EL analyzer. FTIR spectra were recorded in the range of 4000 to 400 cm⁻¹ on an AVATAR 360 Nicolet 380 FT/IR spectrometer using KBr pellets. Thermogravimetric analyses (TGA) were carried out using a Mettler-Toledo TGA/DSC1 in N₂ or air flow, from 25 °C to 350 °C, with a heating rate of 5 °C/min. Powder X-ray diffraction (PXRD) analyses were performed on a Rigaku Dmax-2000

X-ray diffractometer with Cu K α ($\lambda = 1.54059 \text{ \AA}$) radiation. Variable-temperature magnetic susceptibility measurements of **1** and **2** were performed on Quantum Design PPMS magnetometer (100~10 kHz) and Quantum Design SQUID-MPMS3 (1~1 kHz) magnetometer.

Computational details

Complete-active-space self-consistent field (CASSCF) calculations on the Dy³⁺ ion fragments of complexes **1** and **2** on the basis of X-ray determined geometry have been carried out with MOLCAS 8.1 program package. For complex **1**, there are two type of Dy³⁺ ions, the influence of neighboring Dy³⁺ ion was taken into account by diamagnetic Lu. For complex **2**, there is only one type of Dy³⁺ ion, and thus we only need to calculate one Dy³⁺ ion fragment. During the calculations, the other Dy³⁺ ion was replaced by diamagnetic Lu³⁺ ion, the model structure as show in Fig. S16.

For CASSCF calculations, the basis sets for all atoms are atomic natural orbitals from the MOLCAS ANO-RCC library: ANO-RCC-VTZP for Dy³⁺ ion; VTZ for close O and N; VDZ for distant atoms. The calculations employed the second order Douglas-Kroll-Hess Hamiltonian, where scalar relativistic contractions were taken into account in the basis set and the spin-orbit coupling was handled separately in the restricted active space state interaction (RASSI-SO) procedure. For the fragment of Dy³⁺ ion, the active electrons in 7 active spaces include all f electrons CAS (9, 7) for complexes **1** and **2** in the CASSCF calculation. To exclude all the doubts we calculated all the roots in the active space. We have mixed the maximum number of spin-free state which was possible with our hardware (all from 21 sextets, 128 from 224 quadruplets and 130 from 490 doublets for Dy³⁺ ion fragments).

Fitting the exchange interaction in two complexes using Lines model based on CASSCF results

To fit the exchange interaction in complex **1** and **2**, we took two steps to obtain them. Firstly, we calculated one Dy³⁺ ion fragment using CASSCF to obtain the corresponding magnetic properties. Then, the exchange interaction between the magnetic centers is considered within the Lines model,² while the account of the dipole-

dipole magnetic coupling is treated exactly. The Lines model is effective and has been successfully used widely in the research field of f-element single-molecule magnets.⁸

For compound **1** and **2**, there is only one type of J .

The exchange Hamiltonian is:

$$H_{exch} = -J_{total} \hat{S}_{Dy1} \hat{S}_{Dy1A} \quad (S1)$$

The J_{total} is the parameter of the total magnetic interaction ($J_{total} = J_{dipolar} + J_{exchange}$) between magnetic center ions. The $\hat{S}_{Dy} = \pm 1/2$ are the ground pseudospin on the Dy³⁺ ion sites. The dipolar magnetic coupling can be calculated exactly, while the exchange coupling constant was fitted through comparison of the computed and measured magnetic susceptibility and molar magnetization using the POLY_ANISO program.¹⁶

Table S1 Crystallographic data and Structure Refinement for complexes **1** and **2**.

Complex	1	2
Formula	C ₅₁ H ₄₆ Dy ₂ N ₁₂ O ₁₈ Cl ₂	C ₂₃ H ₂₄ DyN ₅ O ₁₁ Cl
Mr	1510.90	744.4
Crystal system	monoclinic	monoclinic
Space group	<i>P n</i>	<i>P 2₁/n</i>
T(K)	100 K	100 K
a(Å)	8.1636 (1)	7.7632(6) Å
b(Å)	21.8109(3)	22.296(2) Å
c(Å)	15.9871(3)	15.2772(9)
<i>a</i> (°)	90	90
<i>β</i> (°)	99.6277(14)	92.035(6)
<i>γ</i> (°)	90	90
<i>V</i> (Å ³)	2806.53(7)	2642.7(3)
Z	2	2
μ (mm ⁻¹)	15.681	3.000
<i>F</i> (000)	1492	1472
GOF	1.056	1.220
Data collected	41391	15764
Unique	9314	5165
R _{int}	0.0687	0.0869
<i>R</i> 1, <i>wR</i> 2 [<i>I</i> >2σ(<i>I</i>)]	0.0440, 0.1176	0.0972, 0.1769
R1, wR2 [all data]	0.0454, 0.1190	0.1275, 0.1275

Table S2 Selected Bond Distances (\AA) in complexes **1** and **2**.

1		1	
Dy1-O1	2.191(4)	Dy2-O2	2.338(0)
Dy1-O2	2.367(3)	Dy2-O3	2.168(5)
Dy1-O4	2.362(5)	Dy2-O4	2.310(3)
Dy1-O6	2.382(1)	Dy2-O5	2.395(5)
Dy1-O7	2.399(1)	Dy2-O8#1	2.402(4)
Dy1-O9	2.354(11)	Dy2-O10#2	2.417(4)
Dy1-N1	2.474(6)	Dy2-N3	2.535(6)
Dy1-N6	2.545(6)	Dy2-N4	2.494(6)
2			
Dy1-O1	2.197(9)		
Dy1-O2	2.390(8)		
Dy1-O2#1	2.316(9)		
Dy1-O3	2.443(9)		
Dy1-O4	2.481(9)		
Dy1-O5#2	2.373(9)		
Dy1-N1	2.463(10)		
Dy1-N3#1	2.604(10)		

Table S3 Relaxation fitting parameters from Least-Squares Fitting of $\chi(f)$ data under zero dc field of 1.

T/K	χ_T	χ_s	α	τ
2	18.32	0.030	0.17	0.41
2.5	14.59	0.029	0.16	0.27
3	12.22	0.027	0.16	0.19
3.5	10.43	0.025	0.16	0.13
4	9.12	0.024	0.16	0.094
4.5	8.05	0.021	0.16	0.064
5	7.24	0.019	0.16	0.044
5.5	6.56	0.014	0.16	0.029
6	5.98	0.012	0.16	0.020
6.5	5.48	0.0089	0.16	0.014
7	5.07	0.0067	0.16	0.010
7.5	4.70	0.0036	0.16	0.0073
8	4.37	0.0066	0.15	0.0054
8.5	4.08	0.011	0.15	0.0040
9	3.83	0.018	0.15	0.0031
9.5	3.60	0.023	0.14	0.0023
10	3.40	0.043	0.14	0.0018
10.5	3.22	0.062	0.13	0.0014
11	3.06	0.087	0.13	0.0012
11.5	2.92	0.11	0.12	9.73E-4
12	2.79	0.15	0.12	8.01E-4
12.5	2.67	0.18	0.11	6.63E-4
13	2.49	0	0.21	5.10E-4
13.5	2.40	0	0.21	4.07E-4
14	2.31	0	0.24	3.23E-4
14.5	2.20	0	0.24	2.54E-4
15	2.12	0	0.25	2.01E-4
15.5	2.04	0	0.25	1.60E-4
16	1.95	0.010	0.25	1.28E-4
16.5	1.87	0.037	0.24	1.02E-4
17	1.80	0.072	0.22	8.45E-5
17.5	1.73	0.11	0.21	7.07E-5
18	1.67	0.17	0.18	6.15E-5
18.5	1.61	0.22	0.16	5.26E-5
19	1.56	0.28	0.13	4.68E-5
19.5	1.51	0.34	0.10	4.09E-5
20	1.47	0.35	0.10	3.48E-5
20.5	1.42	0.39	0.083	3.06E-5
21	1.39	0.42	0.072	2.64E-5
21.5	1.35	0.42	0.068	2.23E-5
22	1.32	0.43	0.062	1.88E-5

Table S4 Relaxation fitting parameters from Least-Squares Fitting of $\chi(f)$ data under zero dc field of 2.

T/K	χ_T	χ_s	α	τ
4	4.65	0.048	0.16	0.45
4.5	3.79	0.046	0.14	0.23
5	3.32	0.043	0.13	0.13
5.5	2.97	0.041	0.12	0.080
6	2.72	0.039	0.12	0.050
6.5	2.48	0.037	0.12	0.032
7	2.27	0.035	0.12	0.021
7.5	2.11	0.035	0.11	0.014
8	1.96	0.033	0.12	0.010
8.5	1.83	0.033	0.11	0.0075
9	1.72	0.033	0.11	0.0055
9.5	1.61	0.034	0.10	0.0041
10	1.52	0.035	0.09	0.0031
10.5	1.44	0.033	0.09	0.0023
11	1.38	0.035	0.09	0.0018
11.5	1.31	0.039	0.09	0.0014
12	1.25	0.039	0.09	0.0011
12.5	1.19	0.054	0.07	9.09E-4
13	1.15	0.047	0.09	7.15E-4
13.5	1.10	0.050	0.09	5.64E-4
14	1.06	0.05	0.09	4.44E-4
14.5	1.02	0.06	0.09	3.53E-4
15	0.99	0.014	0.15	3.03E-4
15.5	0.95	0.014	0.15	2.31E-4
16	0.93	0.0087	0.16	1.78E-4
16.5	0.85	0.023	0.11	1.25E-4
17	0.84	0.019	0.13	9.69E-5
17.5	0.82	0.0099	0.16	7.36E-5
18	0.80	0.011	0.16	5.45E-5
18.5	0.77	0.013	0.16	4.03E-5
19	0.74	0.055	0.11	3.25E-5
19.5	0.73	0.026	0.16	2.27E-5
20	0.70	0.025	0.15	1.71E-5
20.5	0.69	0	0.18	1.17E-5
21	0.67	0.051	0.15	9.96E-6

Table S5 Calculated energy levels (cm^{-1}) and \mathbf{g} (g_x, g_y, g_z) tensors of the lowest Kramers doublets (KDs) of the Dy fragments of complexes **1** and **2**.

KDs	1-Dy1		1-Dy2		2	
	E	\mathbf{g}	E	\mathbf{g}	E	\mathbf{g}
1	0.0	0.002	0.0	0.018	0.0	0.002
		0.003		0.033		0.003
		19.485		19.729		19.808
2	93.4	0.213	179.7	0.247	169.3	0.120
		0.279		0.281		0.589
		16.782		16.945		16.563
3	197.9	3.009	305.2	0.390	201.5	0.002
		5.743		1.378		0.463
		10.272		11.924		18.301
4	219.8	8.041	340.6	2.777	279.2	0.777
		7.175		6.669		1.119
		0.065		10.871		13.894
5	253.1	1.810	406.3	0.799	340.4	5.486
		4.236		3.687		6.565
		11.760		10.557		9.233
6	289.0	8.691	516.9	0.971	411.9	0.513
		6.984		3.671		0.862
		4.350		10.788		13.593
7	357.6	0.809	579.1	1.567	538.7	0.264
		1.349		3.976		0.342
		15.696		14.041		17.495
8	425.8	0.199	699.8	0.082	699.0	0.029
		0.339		0.129		0.050
		17.804		19.432		19.674

Table S6 Fitted exchange coupling constant J_{exch} , the calculated dipole-dipole interaction J_{dipolar} and the total J between Dy^{3+} ions in **1** and **2**. (cm^{-1}).

		1	2
J	J_{dipolar}	4.52	4.37
	J_{exch}	-0.75	-1.5
	J_{total}	3.77	2.87

Table S7 Included angle (θ) between the local main magnetic axis of the ground Kramers doublet and the vector connecting the two Dy³⁺ ions for complex **1** and **2**.

θ	1		2
	Dy1-Dy2	Dy1-Dy2	Dy1-Dy1A
	23.562°	15.164°	21.007°

Table S8 Wavefunction composition for the eight Kramer doublets of the $^6\text{H}_{15/2}$ ground multiplet of complexes **1** and **2**.

KDs	1 (dy_2)
1	0.94 ±15/2⟩
2	0.72 ±13/2⟩+0.12 ±11/2⟩+0.07 ±9/2⟩+0.05 ±5/2⟩
3	0.15 ±13/2⟩+0.10 ±11/2⟩+0.08 ±9/2⟩+0.10 ±7/2⟩+0.23 ±3/2⟩+0.24 ±3/2⟩
4	0.06 ±13/2⟩+0.09 ±11/2⟩+0.04 ±7/2⟩+0.07 ±3/2⟩+0.12 ±3/2⟩+0.54 ±1/2⟩
5	0.11 ±11/2⟩+0.09 ±9/2⟩+0.13 ±7/2⟩+0.23 ±5/2⟩+0.38 ±3/2⟩
6	0.20 ±11/2⟩+0.15 ±7/2⟩+0.32 ±5/2⟩+0.18 ±3/2⟩
7	0.23 ±11/2⟩+0.17 ±9/2⟩+0.16 ±7/2⟩+0.28 ±5/2⟩+0.09 ±3/2⟩
8	0.06 ±11/2⟩+0.43 ±9/2⟩+0.40 ±7/2⟩+0.08 ±5/2⟩
KDs	1 (dy_1)
1	0.97 ±15/2⟩
2	0.84 ±13/2⟩+0.06 ±11/2⟩
3	0.05 ±13/2⟩+0.13 ±11/2⟩+0.17 ±7/2⟩+0.09 ±1/2⟩
4	0.07 ±11/2⟩+0.26 ±9/2⟩+0.09 ±7/2⟩+0.24 ±5/2⟩+0.24 ±3/2⟩+0.06 ±1/2⟩
5	0.13 ±11/2⟩+0.32 ±9/2⟩+0.12 ±7/2⟩+0.08 ±5/2⟩+0.25 ±1/2⟩
6	0.08 ±11/2⟩+0.18 ±9/2⟩+0.31 ±7/2⟩+0.09 ±5/2⟩+0.10 ±3/2⟩+0.08 ±1/2⟩
7	0.07 ±11/2⟩+0.18 ±9/2⟩+0.10 ±7/2⟩+0.25 ±5/2⟩+0.16 ±3/2⟩+0.21 ±1/2⟩
8	0.08 ±9/2⟩+0.12 ±7/2⟩+0.20 ±5/2⟩+0.28 ±3/2⟩+0.29 ±1/2⟩
KDs	2 (dy_1)
1	0.99 ±15/2⟩
2	0.78 ±13/2⟩+0.13 ±11/2⟩
3	0.05 ±13/2⟩+0.12 ±9/2⟩+0.12 ±7/2⟩+0.19 ±5/2⟩+0.20 ±3/2⟩+0.25 ±1/2⟩
4	0.13 ±13/2⟩+0.47 ±11/2⟩+0.19 ±9/2⟩+0.15 ±7/2⟩
5	0.16 ±11/2⟩+0.22 ±9/2⟩+0.14 ±7/2⟩+0.23 ±5/2⟩+0.10 ±3/2⟩+0.11 ±1/2⟩
6	0.11 ±11/2⟩+0.22 ±9/2⟩+0.20 ±7/2⟩+0.14 ±5/2⟩+0.19 ±3/2⟩+0.11 ±1/2⟩
7	0.10 ±9/2⟩+0.16 ±7/2⟩+0.19 ±5/2⟩+0.22 ±3/2⟩+0.29 ±1/2⟩
8	0.05 ±11/2⟩+0.12 ±9/2⟩+0.17 ±7/2⟩+0.21 ±5/2⟩+0.20 ±3/2⟩+0.20 ±1/2⟩

Table S9 The *CShM* values calculated by *SHAPE 2.0* for **1** and **2**.

Coordination Geometry	1-Dy1	1-Dy2	2
Triangular dodecahedron(D_{2d})	2.887	3.209	3.153
Biaugmented trigonal prism J50(C_{2v})	3.655	2.339	1.925
Biaugmented trigonal prism (C_{2v})	2.416	2.236	1.068

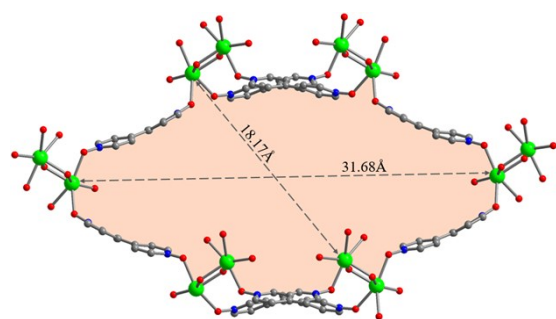


Fig. S1 coordination polyhedron around Dy1 and Dy2 of **1**.

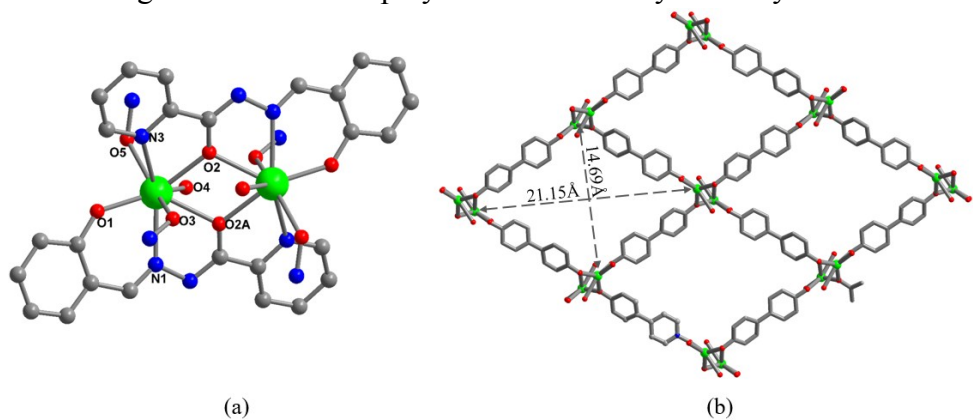


Fig. S2 The dinuclear unit (a) and 2D layer (b) of **2**.

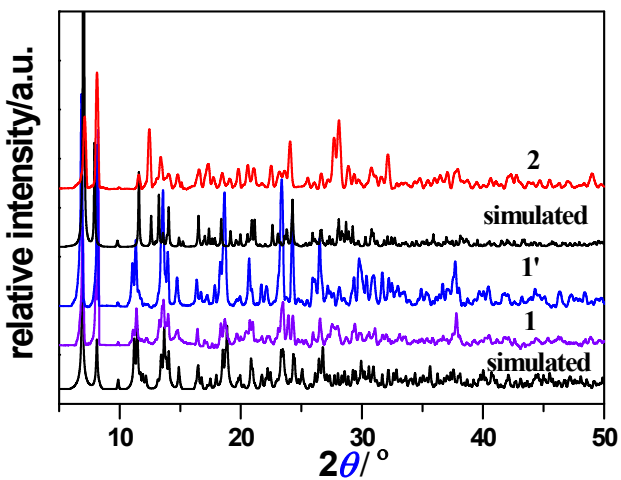


Fig. S3 Powder X-ray diffraction profiles of **1**, **1'** and **2** together with a simulation from the single crystal data (**1'** can be obtained by exposing **2** to a mixture vapor of methanol and acetonitrile in a ratio of one to nine for six days).

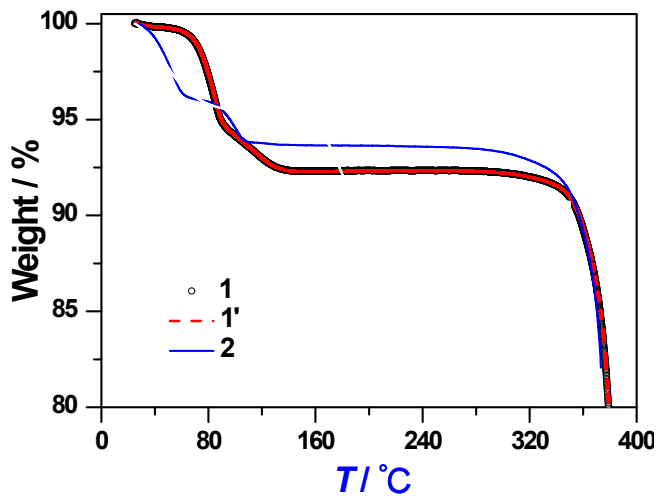


Fig. S4 TGA curves of complexes **1**, **2** and **1'**.

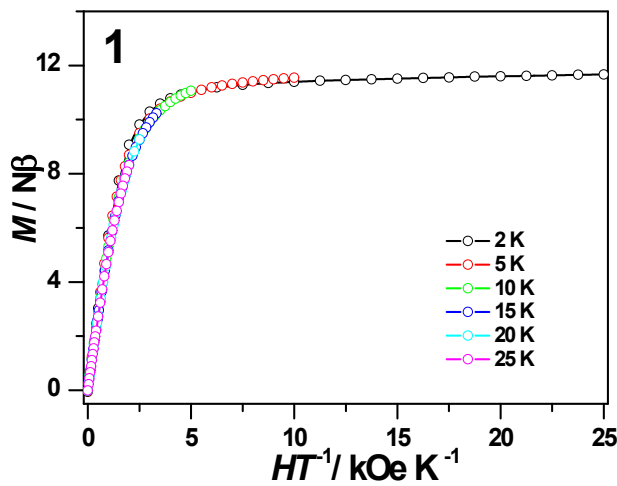


Fig. S5 Plots of M - H for **1**.

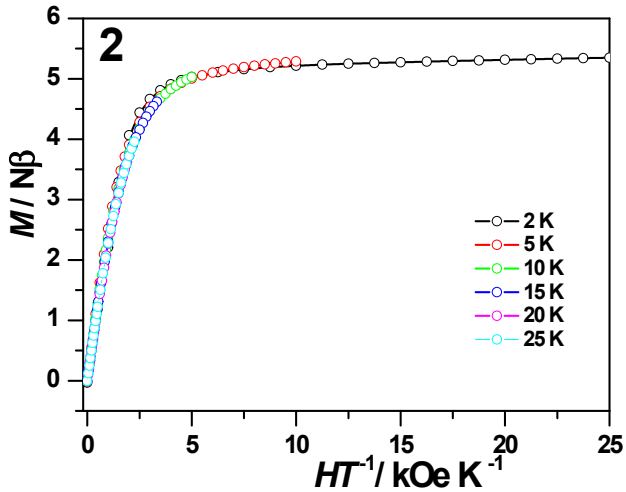


Fig. S6 Plots of M - H for **2**.

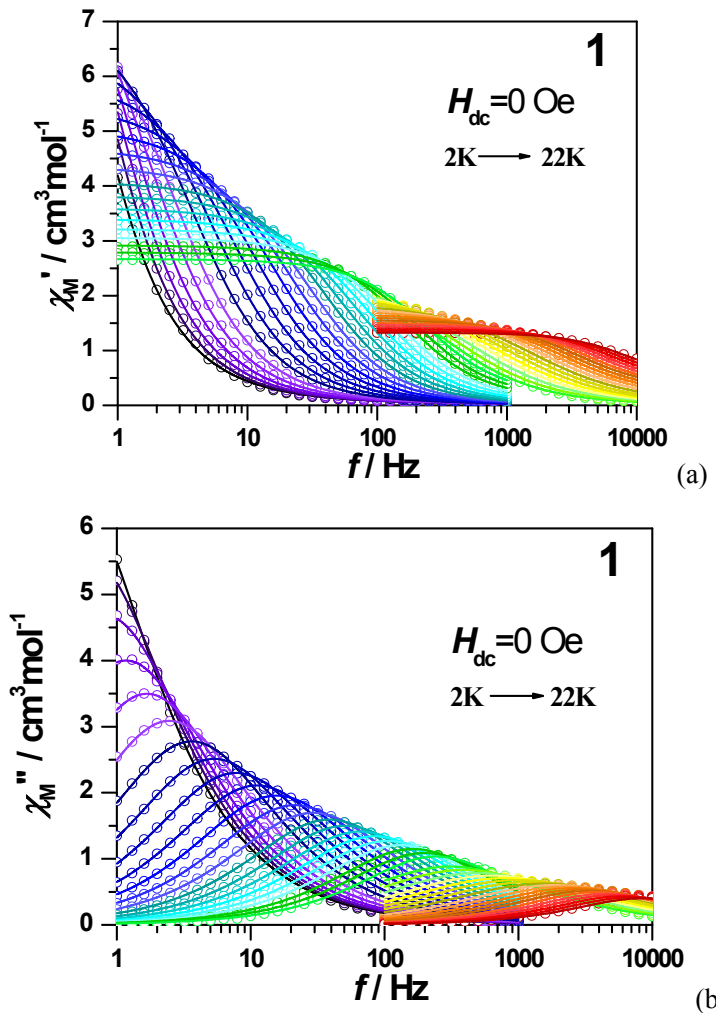


Fig. S7 Ac - f curves measured under zero dc fields for **1**. Solid lines were fitted using a generalized Debye relaxation model, simultaneously to $\chi'(f)$ and $\chi''(f)$ curves.

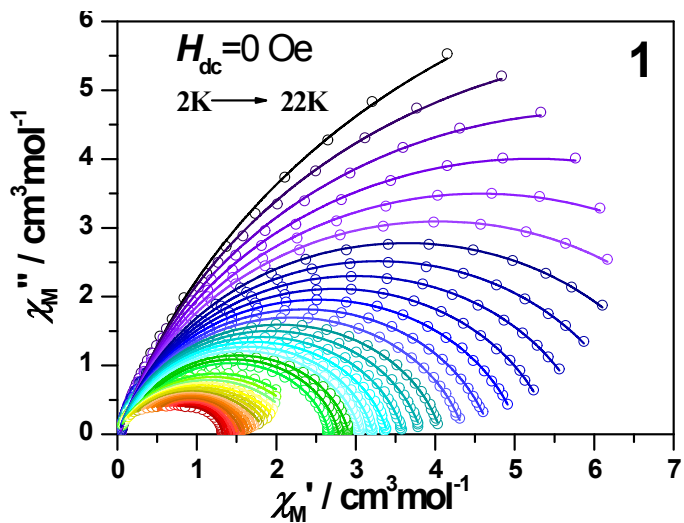


Fig. S8 Cole-cole plots of **1** under zero *dc* field.

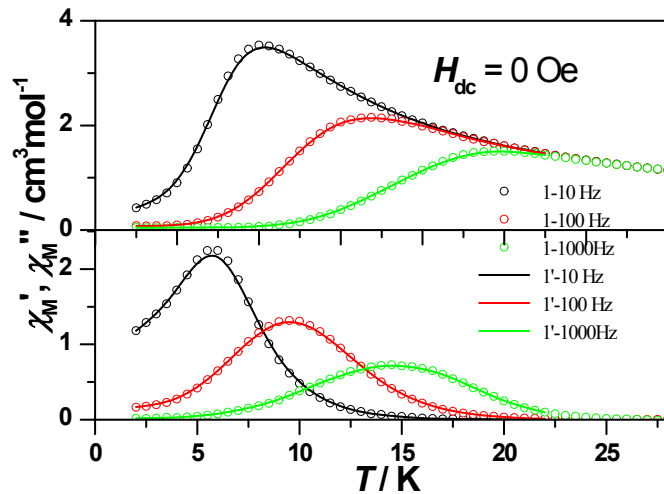
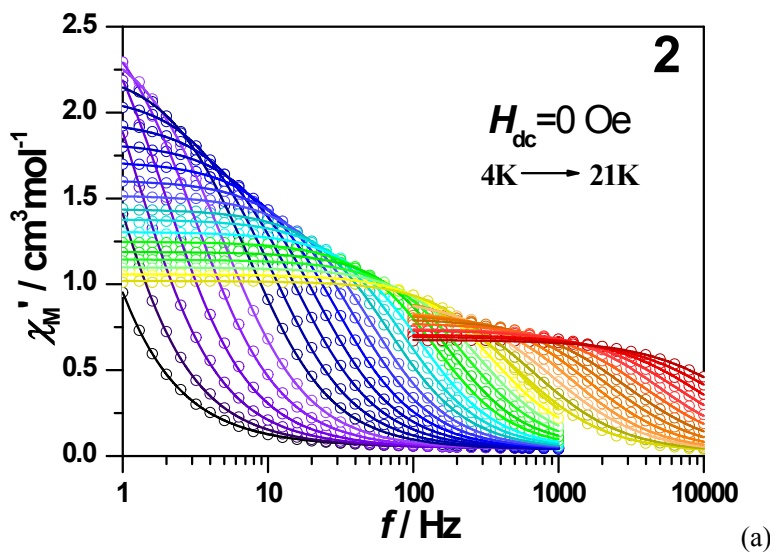


Fig. S9 Temperature dependence of the in-phase χ_M' (top) and out-of-phase χ_M'' (bottom) ac signals at 10Hz, 100 Hz and 1000 Hz under zero dc field for **1** and **1'**.



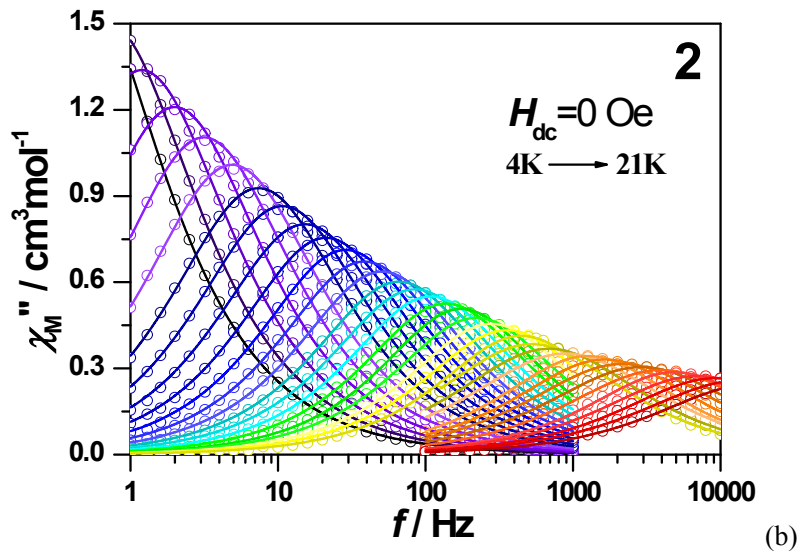


Fig. S10 $Ac-f$ curves measured under zero dc fields for **2**. Solid lines were fitted using a generalized Debye relaxation model, simultaneously to $\chi'(f)$ and $\chi''(f)$ curves.

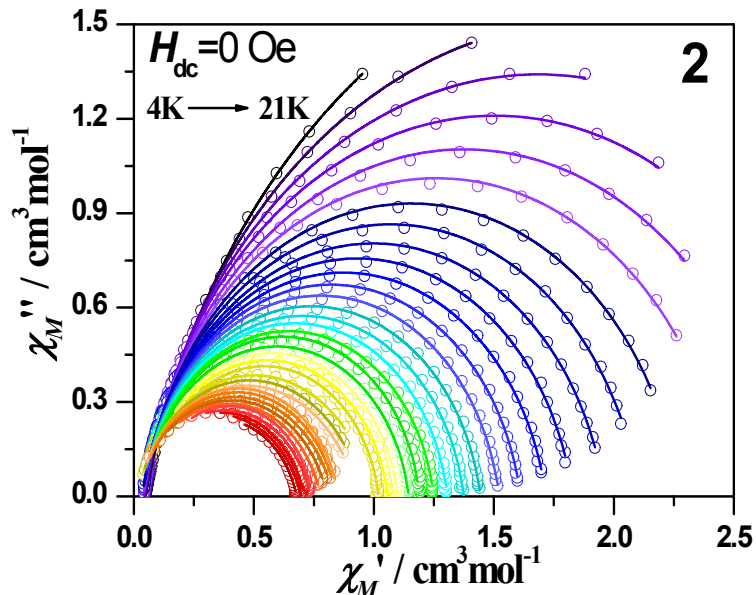


Fig. S11 Cole-cole plots of **2** under zero dc field. zero dc field.

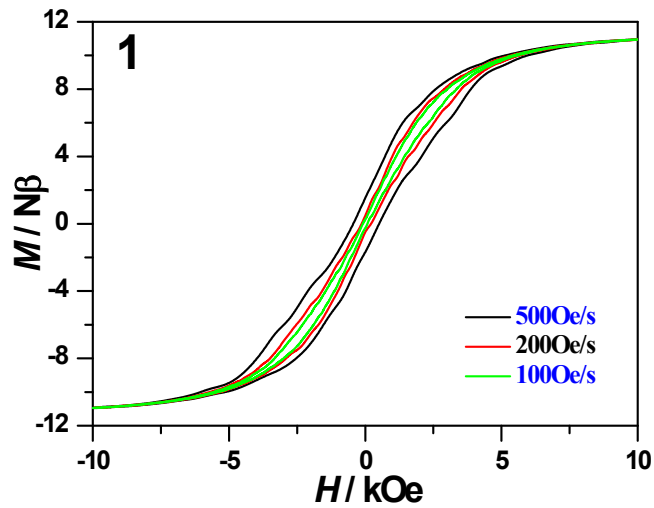


Fig. S12 Hysteresis loop for **1** measured with different sweep rates at 2 K.

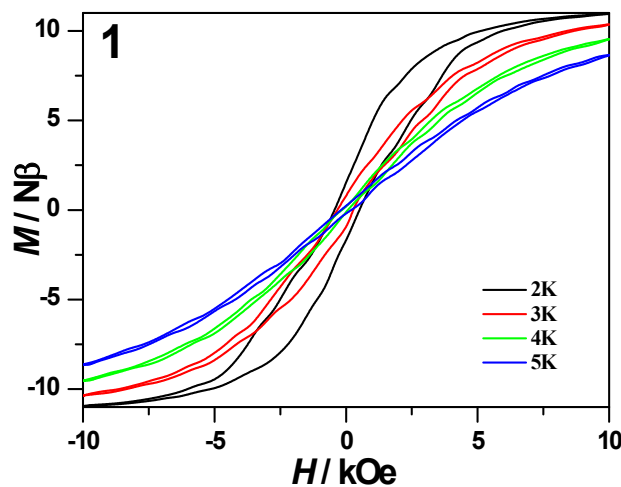


Fig. S13 Hysteresis loop for **1** measured at different temperatures with sweep rates of 500 Oe/s.

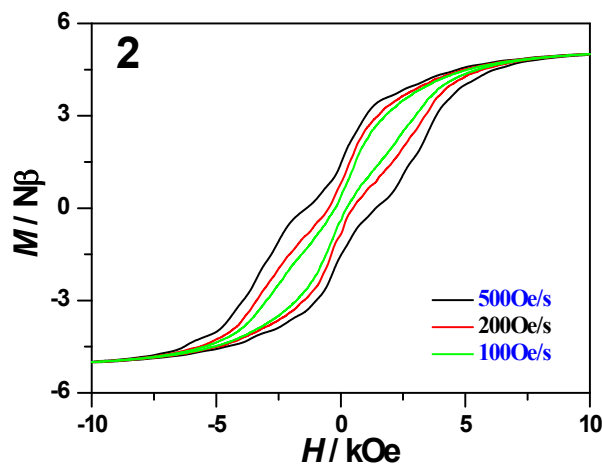


Fig. S14 Hysteresis loop for **2** measured with different sweep rates at 2 K.

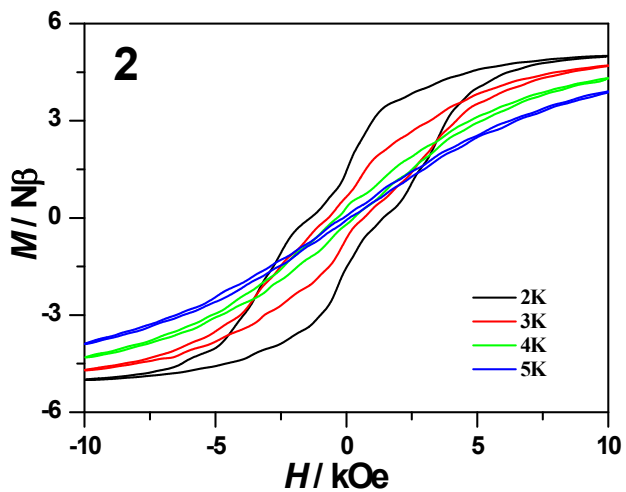


Fig. S15 Hysteresis loop for **2** measured at different temperatures with sweep rates of 500 Oe/s.

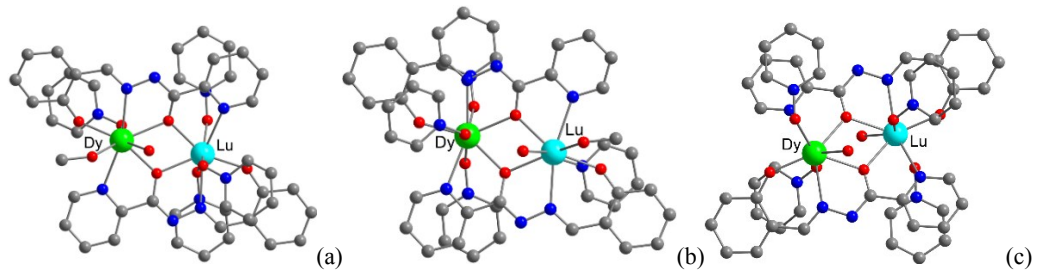


Fig. S16 Calculated model structure for complex **1** (a, b) and **2** (c); H atoms are omitted.

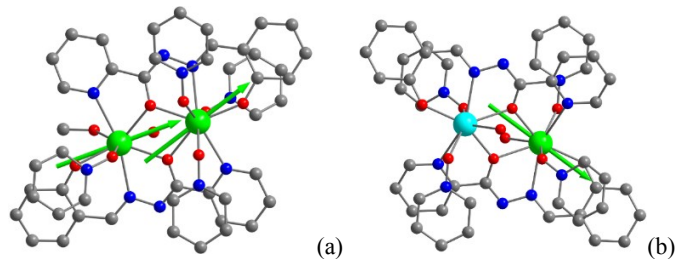


Fig. S17 Orientation of the local main magnetic axes of the ground Kramers doublet on Dy³⁺ ion of complexes **1** (a) and **2** (b).

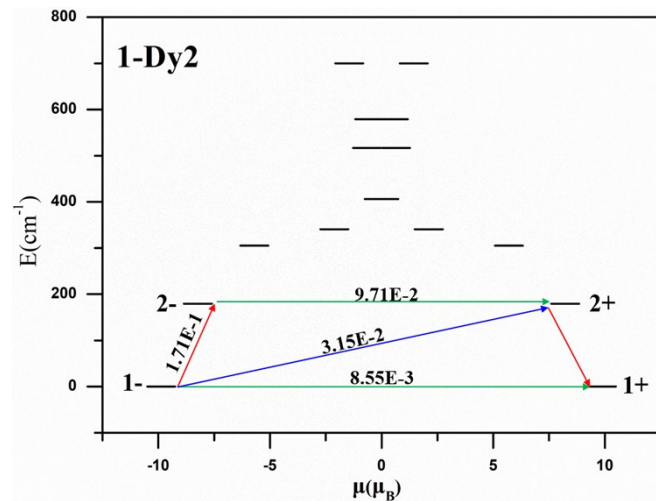


Fig. S18 The magnetization blocking barriers of **1-Dy2**. The thick black lines represent the Kramers doublets as a function of their magnetic moment along the magnetic axis. The green lines correspond to diagonal quantum tunneling of magnetization (QTM); the blue line represent off-diagonal relaxation process. The numbers at each arrow stand for the mean absolute value of the corresponding matrix element of transition magnetic moment.